Front. Phys. 10, 106802 (2015)
DOI 10.1007/s11467-015-0467-z

RESEARCH ARTICLE

Epitaxial growth and thermostability of cubic and hexagonal $SrMnO_3$ films on $SrTiO_3(111)$

Rui-Nan Song[1,2], Min-Hui Hu[2], Xiang-Rong Chen[1,3], Jian-Dong Guo[2,4,†]

[1] *Institute of Atomic and Molecular Physics, College of Physical Science and Technology, Sichuan University, Chengdu 610065, China*

[2] *Institute of Physics, Chinese Academy of Sciences, Beijing 100190, China*

[3] *Key Laboratory of High Energy Density Physics and Technology of Ministry of Education, Sichuan University, Chengdu 610064, China*

[4] *Collaborative Innovation Center of Quantum Matter, Beijing 100871, China*

Corresponding author. E-mail: †jdguo@iphy.ac.cn

Received February 4, 2015; accepted March 13, 2015

The growth of $SrMnO_3$ films on $SrTiO_3(111)$ substrates by pulsed laser deposition was studied and found to produce cubic and hexagonal (4H) structures in the $SrMnO_3$ films. By adjusting the substrate temperature and oxygen pressure, the stability of the two phases was fine-tuned, resulting in the growth of cubic-$SrMnO_3(111)$ or 4H-$SrMnO_3(0001)$ film, with the 4H phase being the more stable at room temperature and ambient pressure in the bulk form. The growth temperature of the cubic phase was also further lowered relative to the bulk thermodynamics by strain at the heterointerface, and once obtained, it was stable at temperatures of up to 800 °C.

Keywords oxide film, pulsed laser deposition, heteroepitaxy, $SrMnO_3$

PACS numbers 68.55.aj, 68.35.Rh, 81.15.Fg

1 Introduction

Thin films of [111]-oriented perovskite oxides ABO_3 (where A and B are metal cations) have attracted extensive attention of late because of their peculiar physical properties [1–3], such as the fact that the six-fold symmetry of their honeycomb structure can result in novel topology states at their surfaces or interfaces [4, 5]. In addition, [111]-oriented superlattices allow for the design and construction of long-range ordering of cation dopants. One example of this is the double perovskite La_2FeCrO_6 structure with B site cations (Fe and Cr) distributed alternatively along the ⟨001⟩ direction that has been obtained by growing a $LaFeO_3/LaCrO_3(111)$ superlattice [6, 7], which was found to have magnetic properties distinctly different from a disordered solid solution of $LaFeO_3$ and $LaCrO_3$. An exchange bias has also been unexpectedly discovered [8] in the [111]-oriented superlattice of paramagnetic $LaNiO_3$ and ferromagnetic $LaMnO_3$. Meanwhile, in the perovskite $AMnO_3$ manganite, A-site doping has been proven effective in tuning the properties of the material by inducing a rich phase diagram that includes colossal magnetoresistance and ferromagnetism [9, 10]. Normally, these cation dopants are randomly distributed and produce a localization effect that reduces the metallicity of electron transport in low-dimensional manganite structures; this is one of the possible reasons for the so-called "deadlayer" problem in $La_{2/3}Sr_{1/3}MnO_3$ ultrathin films [11]. Thus, a [111]-oriented $LaMnO_3/SrMnO_3$ superlattice in which La and Sr are distributed alternatively with long-range ordering along all ⟨100⟩ directions offers a realistic potential to solve this problem by suppressing the localization effect originating from A-site disorder.

It is quite challenging to grow perovskite (111) thin films due to their strong surface polarity and the multiple competing phases in the lattice structure. For example, $SrMnO_3$ is commonly synthesized in either cubic (C) or hexagonal (4H) structures (Fig. 1), both of which are antiferromagnetic insulators with respective Neel temperatures (T_N) of 240 and 280 K [12–14]. The 4H-$SrMnO_3$ structure is made up of alternating face-sharing and corner-sharing MnO_6 molecules along the [0001] orientation [Fig. 1(b)], which contribute to long-range antiferromagnetic ordering [13–15]. The lattice structure of C-$SrMnO_3$, on the other hand, is quite simple [Fig. 1(a)], though first-principles calculations have

shown that strain could produce a multiferroic phase due to its strong spin–phonon coupling [16]. It is important to control the phase of $SrMnO_3$ during its growth, as otherwise, its properties can be quite varied. The stability of the perovskite structure can generally be described by the tolerance factor: $t = \frac{r_A+r_O}{\sqrt{2}(r_B+r_O)}$, where r represents the ionic radii of A and B cations, and O atoms. For $SrMnO_3$ the value of t is 1.04, meaning that the 4H phase is normally stable at room temperature and ambient pressure [17], whereas the cubic phase can only be obtained in a metastable state [13, 15]. In 1970, Negas and Roth [18] presented a phase diagram for bulk $SrMnO_{3-x}$ that demonstrated 4H-$SrMnO_3$ is stable in air up to about 1035 °C. Higher temperatures were shown to induce the formation of oxygen vacancies (V_Os), resulting in a deformation of the 4H phase that causes the crystal to transform into a perovskite-like structure at >1400 °C. By annealing in air at 300 °C for several hours, this perovskite-like $SrMnO_3$ was oxidized to form the cubic phase [13–15, 19].

For thin film growth, 1400 °C is an impractically high temperature and is likely to deteriorate the desired [111]-oriented superlattice by causing serious interdiffusion across the interfaces. With a perovskite (001) substrate, the growth of a 4H-$SrMnO_3$ film can be suppressed by the symmetry mismatch, allowing the cubic phase to be obtained by pulsed laser deposition (PLD) at a reduced temperature of 800 °C [20]. Conversely, with a perovskite (111) surface, the competition between 4H (0001) and cubic (111) cannot be tuned by symmetry alone. This paper therefore looks at introducing an appropriate strain to the heteroepitaxial growth of $SrMnO_3$ films by using $SrTiO_3$(111) as the substrate. These single-crystalline $SrMnO_3$ films are grown by PLD as either a 4H or cubic phase depending on the growth parameters used. In this way, a C-$SrMnO_3$(111) film can be obtained at a temperature as low as 875 °C, which represents a significant reduction when compared to bulk synthesis. This interface epitaxial stabilization also ensures that a C-$SrMnO_3$ film grown on $SrTiO_3$(111) has a good thermostability.

2 Experiments

Films of $SrMnO_3$ were deposited on Nb-doped (0.7 wt.%) $SrTiO_3$(111) single-crystalline substrates (3×12×0.5 mm^3) by ultra-high vacuum PLD using a 248 nm KrF excimer laser (CompexPro201F). Prior to deposition, the substrates were treated by Ar^+ ion sputtering (10 μA/1 KV) for 10 minutes followed by annealing at 900 °C under 3×10^{-6} mbar of oxygen pressure for 1 hour. This resulted in a 4×4 surface reconstruction with a slight Sr accumulation, which effectively stabilizes the $SrTiO_3$(111) polar surface [21]. The samples were then heated by passing a direct current through the substrates, during which time the temperature was monitored by an infrared pyrometer. All depositions were carried out using a laser repetition rate of 2 Hz and an energy density of 1.5 J/cm^2. To control the phase of the $SrMnO_3$ film, the substrate temperature (T_S) and oxygen pressure (P_O) were adjusted to within 850–1000 °C and 2×10^{-6}–5×10^{-3} mbar, respectively. The film thickness was ~60 nm for all samples, based on which it is considered reasonable to exclude any effect of substrate surface reconstruction on the film growth. The samples were post-annealed in a tube furnace at 300 °C under an oxygen flow of ~1 bar to minimize the oxygen vacancies formed. The crystalline structure of the film was characterized by X-ray diffraction (XRD) using an UltimaIV X-ray diffractometer with Cu K radiation ($\lambda = 1.5405$ Å). The DC magnetic susceptibilities were measured between 400 and 10 K by a commercial SQUID-vibrating sample magnetometer (Model S-VSM of Quantum Design) with zero-field cooling.

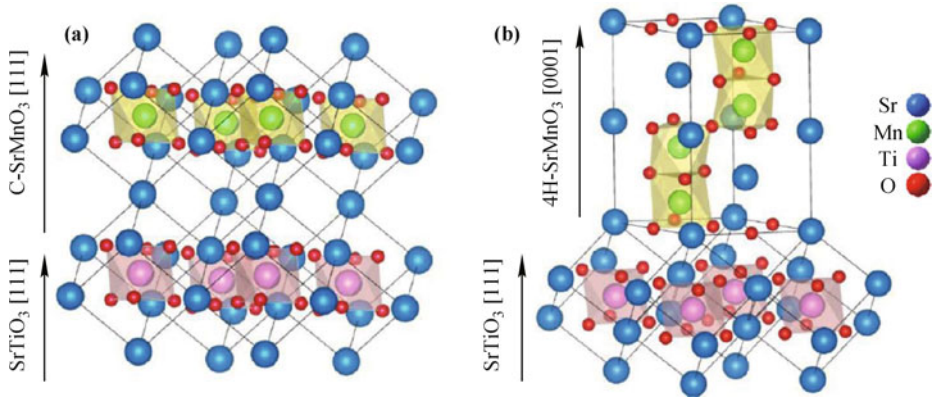

Fig. 1 The structural models of **(a)** cubic- and **(b)** 4H-$SrMnO_3$ on $SrTiO_3$(111) substrate. The perovskite [111] orientation is reserved in the cubic-$SrMnO_3$, while the 4H [0001] orientation accommodates the heteroepitaxy.

3 Results and discussion

The structure of the $SrMnO_3$ films produced on $SrTiO_3$(111) substrates was controlled to be either a 4H or cubic phase by changing the T_S and P_O during growth. Figure 2 shows the XRD spectra of samples deposited at 920 °C/3.3×10^{-5} mbar and 950 °C/4.0×10^{-3} mbar, in which the their different phases can be clearly distinguished. That is, if the diffraction peaks of the substrate are ignored, then one sample shows sharp peaks at $2\theta = 41.06°$ and 89.03° that correspond to the (111) and (222) lattice plane interspacings of C-$SrMnO_3$ (JCPDS Card No. 231413) [22] respectively, while the other shows peaks at $2\theta = 19.57°$ and 61.37° that can be attributed to the (0002) and (0006) interspacings of the 4H phase (JCPDS Card No. 841612) [13], respectively. No other diffractions are detected, indicating that monophased single-crystalline C- or 4H-$SrMnO_3$ films were obtained.

Table 1 summarizes the XRD data of samples grown under different T_S and P_O conditions, and indicates that a high T_S and low P_O favor the formation of the cubic phase, while a low T_S and high P_O lead to a 4H phase. This can be understood through thermodynamic analysis by considering the competition between the 4H and cubic phases to be a chemical process of

$$(SrMnO_3)_{4H} \leftrightarrow (SrMnO_{3-x})_{cubic} + \frac{x}{2}O_2. \quad (1)$$

Oxygen vacancies are involved here since previous study of bulk $SrMnO_3$ has shown them to play a key role in the deformation of 4H-$SrMnO_3$ at temperatures above 1400 °C [18]. In the present study, the V_Os density during film growth is controlled by adjusting P_O, and the T_S and P_O required for transformation from 4H- to C-$SrMnO_3$ should follow the relation [23]:

$$\ln\frac{P_O}{p_0} = -\frac{2\Delta H}{nRT_S} + C_0, \quad (2)$$

where $p_0 = 1$ bar is the standard pressure, $\Delta H = H_{cubic} - H_{4H}$ is the standard enthalpy change (independent of T_S), R is the ideal gas constant, n is the total particle number, and C_0 is a constant. The boundary between C- and 4H-$SrMnO_3$ should therefore appear as a straight line in a phase diagram plot of $1/T_S$ vs. $\lg P_O$ [24], and the slope of this line should be negative given that $\Delta H > 0$ [25, 26]. As shown schematically in Fig. 3, reducing the growth temperature of the C-$SrMnO_3$ film should be accompanied by a decrease in oxygen pressure; the minimum value being limited by the oxidation requirements of oxide growth. Putting the experimentally determined values of T_S and P_O needed to grow C- and 4H-$SrMnO_3$ films into the $1/T_S$ vs. $\lg P_O$ plot, we find that these two phases are indeed separated by a straight line that is consistent with Eq. (2). It is also worth noting here that as the 4H phase is thermodynamically stable, it is reasonable to assume that the growth parameters of the cubic phase would be close to this boundary.

The temperature and P_O required for the transformation between cubic and 4H phases in the bulk material (1400 °C / 0.2 bar) [18] are also labeled in Fig. 3; and

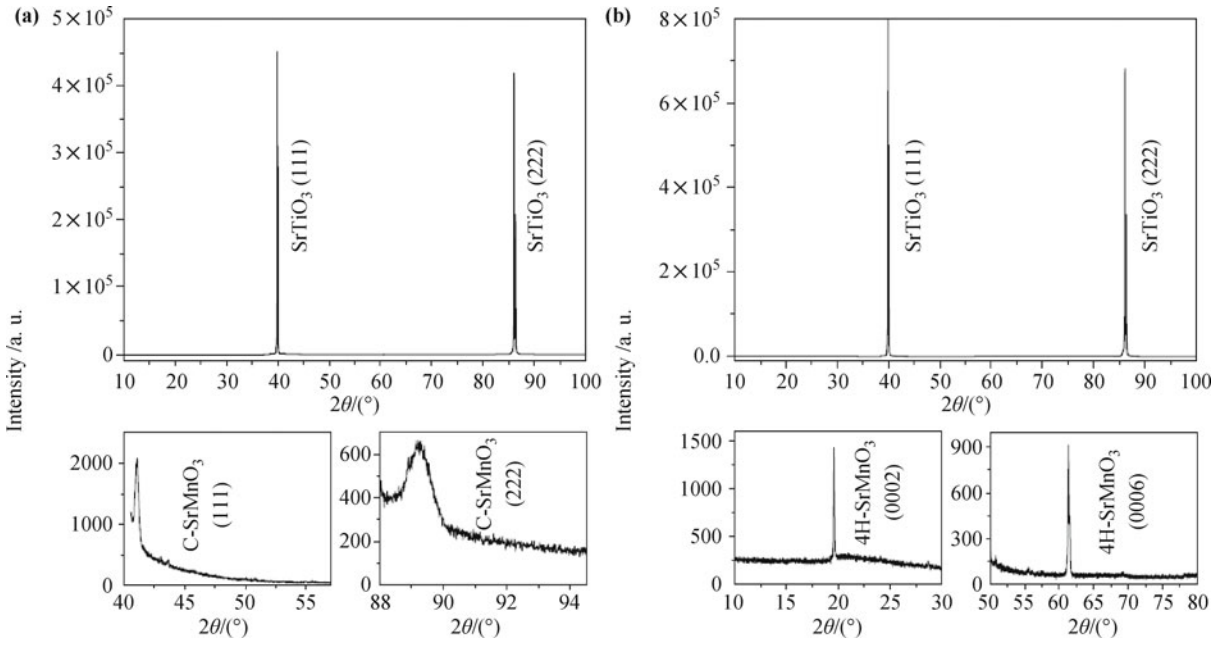

Fig. 2 **(a)** XRD spectrum of C-$SrMnO_3$(111) and **(b)** 4H-$SrMnO_3$(0001) films on $SrTiO_3$(111) substrate. The lower panels show the zoom-in features of the two phases, respectively.

Table 1 XRD results of the $SrMnO_3$ films grown at different temperature and oxygen pressure. The standard lattice interspacing of the cubic [111] (JCPDS card No. 231413 [13]) and 4H [0001] (JCPDS card No. 841612 [23]) are provided for reference.

Sample	T_S/°C	P_O/mbar	d[111]/Å (cubic)	d[222]/Å (cubic)	d[0002]/Å (4H)	d[0006]/Å (4H)	Vertical strain (Δ, %)
1	1000	2.0×10^{-3}	2.1950	1.0959			0.15
2	920	3.3×10^{-5}	2.1966	1.0956			0.12
3	920	2.6×10^{-6}	2.1926	1.0971	\	\	0.15
4	900	5.0×10^{-6}	2.1930	1.0969	\	\	0.15
5	875	5.0×10^{-6}	2.1888	1.0948	\	\	0.34
6	950	4.0×10^{-3}			4.5195	1.5107	0.21
7	866	1.0×10^{-3}	\	\	4.5198	1.5085	0.28
8	900	5.0×10^{-3}	\	\	4.5274	1.5100	0.14
9	850	1.7×10^{-3}	\	\	4.5324	1.5108	0.061
JCPDS card No. 231413	\	\	2.1960	1.0986	\	\	\
JCPDS card No. 841612	\	\	\	\	4.5352	1.5117	\

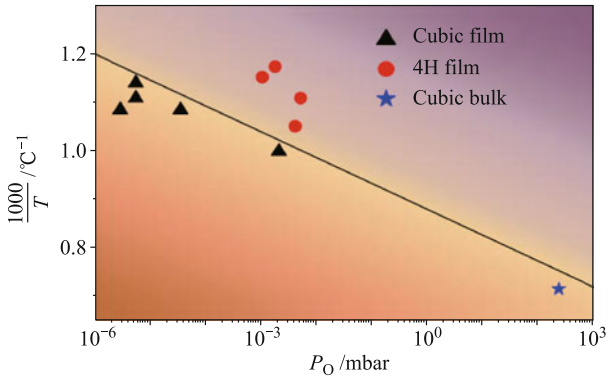

Fig. 3 The phase diagram of $SrMnO_3$. The scattered symbols indicate the growth parameters of the films. The straight line schematically shows the boundary between cubic and 4H phases.

as can be seen, both these parameters fall well below the line for film growth. This indicates that the growth of C-$SrMnO_3$(111) film is possible at lower temperatures than those prescribed by thermodynamics. In the $SrMnO_3/SrTiO_3$ heteroepitaxial structure, any interface strain induced by the lattice mismatch must also be considered. The in-plane lattice mismatch between C-$SrMnO_3$ (space group $Pm\bar{3}m$, a = 3.804 Å) and the $SrTiO_3$ substrate (space group $Pm\bar{3}m$, a = 3.905 Å) is 2.655%, but drops to 1.443% when 4H-$SrMnO_3$(0001) (space group $P6_3/mmc$, a = 5.4434 Å, c = 9.0704 Å) is grown on $SrTiO_3$(111) (see Fig. 1). When formed on $SrTiO_3$(111), either phase of $SrMnO_3$ will experience a compressive strain along its growth direction, but this is expected to be much larger in the case of the cubic phase due to its greater in-plane lattice mismatch. The experimentally observed vertical strain; which is defined as $\Delta = \frac{d-d_{JCPDS}}{d_{JCPDS}}$, where d is the lattice interspacing determined by XRD and d_{JCPDS} is the standard JCPDS card value (No. 231413 [22] and No. 841612 [13]) of the according interspacing; does not, however, show any significant difference between the two phases (Table 1). This may be attributed to the different lattice response of the [111] direction to distortion along [$\bar{1}$01] in the cubic phase when compared to the response of the [0001] direction to distortion along [11$\bar{2}$0] in the 4H phase. Consequently, the stability of the cubic phase is enhanced at the heterointerfaces, allowing film growth at lower temperatures.

Figure 4 shows the susceptibility χ of the cubic and 4H phase films at temperatures of between 10 and 400 K. Both curves exhibit antiferromagnetic phase transitions, with a T_N at 38 K and 41 K for the C- and 4H-$SrMnO_3$ films, respectively. The existence of defects or domain boundaries in the films might be the reason for this being lower than their respective bulk materials [27].

The thermostability of the C-$SrMnO_3$ film was evaluated by annealing it at 800 °C for 8 hours under an

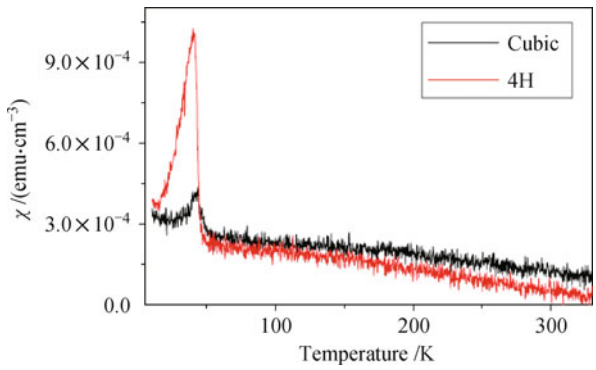

Fig. 4 The susceptibility χ of the films at different temperature measured with zero-field cooling.

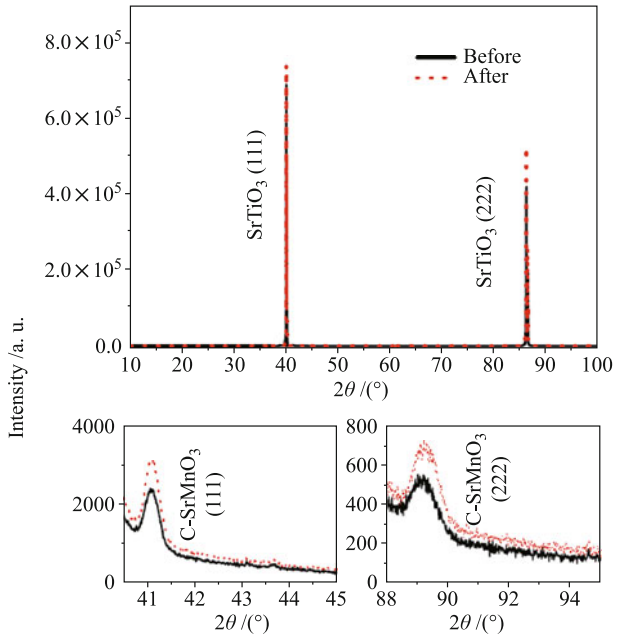

Fig. 5 XRD spectra of the cubic-$SrMnO_3$(111) film before and after annealing at 800 °C for 8 hours in an oxygen flow of ∼1 bar. The lower panels show the zoom-in features.

oxygen flow of ∼1 bar. As shown in Fig. 5, the XRD peaks corresponding to the cubic lattice structure showed no decay or displacement after annealing, indicating that no impurities were formed and the transformation to a 4H phase was inhibited. It is clear from this that thanks to the stabilizing effect of the heteroepitaxial interface cubic-$SrMnO_3$ films should be capable of surviving conditions typical of oxide film growth. They therefore have the potential to provide a reliable template for the design and construction of artificial perovskite superlattices.

4 Conclusion

High-quality $SrMnO_3$ films have been successfully grown on $SrTiO_3$(111) substrates as either a cubic or 4H phase, the resulting structure being controlled by the substrate temperature and oxygen pressure during PLD growth. Following the principal of thermodynamics, the growth temperature of the cubic $SrMnO_3$(111) film is significantly lowered by the strain that is induced by the lattice mismatch at the heterointerfaces. This enhances the thermostability of the cubic-$SrMnO_3$ film, giving it the potential to be used for consistent growth of artificial perovskite superlattices.

Acknowledgements This work was supported by the National Basic Research Program of Ministry of Science and Technology of China (Grant No. 2012CB921700), the National Natural Science Foundation of China (Grant No. 11225422), and the Strategic Priority Research Program (B) of CAS (Grant No. XDB07010100). J. Guo is grateful for the support of the External Cooperation Program of BIC, CAS (Grant No. 112111KYSB20130007).

References and notes

1. J. Heber, Materials science: Enter the oxides, *Nature* 459(7243), 28 (2009)
2. D. G. Schlom, L.-Q. Chen, X. Pan, A. Schmehl, and M. A. Zurbuchen, A thin film approach to engineering functionality into oxides, *J. Am. Ceram. Soc.* 91(8), 2429 (2008)
3. M. Johnsson and P. Lemmens, Perovskites and thin films-crystallography and chemistry, *J. Phys.: Condens. Matter* 20(26), 264001 (2008)
4. D. Xiao, W. Zhu, Y. Ran, N. Nagaosa, and S. Okamoto, Interface engineering of quantum Hall effects in digital transition metal oxide heterostructures, *Nat. Commun.* 2, 596 (2011)
5. Y. Wang, Z. Wang, Z. Fang, and X. Dai, Interaction-induced quantum anomalous Hall phase in (111) bilayer of $LaCoO_3$, arXiv: 1409.6797 (2014).
6. B. Gray, H. N. Lee, J. Liu, J. Chakhalian, and J. W. Freeland, Local electronic and magnetic studies of an artificial La_2FeCrO_6 double perovskite, *Appl. Phys. Lett.* 97(1), 013105 (2010)
7. K. Ueda, H. Tabata, and T. Kawai, Ferromagnetism in $LaFeO_3$–$LaCrO_3$ superlattices, *Science* 280(5366), 1064 (1998)
8. M. Gibert, P. Zubko, R. Scherwitzl, J. Iñiguez, and J. M. Triscone, Exchange bias in $LaNiO_3$–$LaMnO_3$ superlattices, *Nat Mater* 11(3), 195 (2012)
9. E. Dagotto, T. Hotta, and A. Moreo, Colossal magnetoresistant materials: The key role of phase separation, *Phys. Rep.* 344(1), 1 (2001)
10. A. M. Haghiri-Gosnet and J. P. Renard, CMR manganites: Physics, thin films and devices, *J. Phys. D: Appl. Phys.* 36(8), R127 (2003)
11. M. Huijben, L. W. Martin, Y. H. Chu, M. B. Holcomb, P. Yu, G. Rijnders, D. H. A. Blank, and R. Ramesh, Critical thickness and orbital ordering in ultrathin $La_{0.7}Sr_{0.3}MnO_3$ films, *Phys. Rev. B* 78(9), 094413 (2008)
12. R. Søndenå, P. Ravindran, S. Stølen, T. Grande, and M. Hanfland, Electronic structure and magnetic properties of cubic and hexagonal $SrMnO_3$, *Phys. Rev. B* 74(14), 144102 (2006)
13. P. D. Battle, T. C. Gibb, and C. W. Jones, The structural and magnetic properties of $SrMnO_3$: A reinvestigation, *J. Solid State Chem.* 74(1), 60 (1988)
14. A. A. Belik, Y. Matsushita, Y. Katsuya, M. Tanaka, T. Kolodiazhnyi, M. Isobe, and E. Takayama-Muromachi, Crystal

structure and magnetic properties of 6H–$SrMnO_3$, *Phys. Rev. B* 84(9), 094438 (2011)

15. I. N. González-Jiménez, A. Torres-Pardo, A. E. Sánchez-Peláez, Á. Gutiérrez, M. García-Hernández, J. M. González-Calbet, M. Parras, and Á. Varela, Synthesis of 4H–$SrMnO_{3.0}$ nanoparticles from a molecular precursor and their topotactic reduction pathway identified at atomic scale, *Chem. Mater.* 26(7), 2256 (2014)
16. J. H. Lee and K. M. Rabe, Epitaxial-strain-induced multiferroicity in $SrMnO_3$ from first principles, *Phys. Rev. Lett.* 104(20), 207204 (2010)
17. V. M. Goldschmidt, Die Gesetze der Krystallochemie, *Naturwissenschaften* 14(21), 477 (1926)
18. T. Negas and R. S. Roth, The system $SrMnO_{3-x}$, *J. Solid State Chem.* 1(3), 409 (1970)
19. A. Sacchetti, M. Baldini, P. Postorino, C. Martin, and A. Maignan, Raman spectroscopy on cubic and hexagonal $SrMnO_3$, *Journal of Raman Spectroscopy* 37(5), 591 (2006)
20. S. Kobayashi, Y. Tokuda, T. Ohnishi, T. Mizoguchi, N. Shibata, Y. Sato, Y. Ikuhara, and T. Yamamoto, Cation off-stoichiometric $SrMnO_3$ thin film grown by pulsed laser deposition, *J. Mater. Sci.* 46(12), 4354 (2010)
21. J. Feng, X. Zhu, and J. Guo, Reconstructions on $SrTiO_3$(111) surface tuned by Ti/Sr deposition, *Surf. Sci.* 614, 38 (2013)
22. National Bureau of Standards Monograph 25, Section 10–Data for 84 Substances, 58 (1972)
23. R. A. Alberty and R. J. Silbey, *Physical Chemistry*, 3rd Ed., John Wiley &Sons, Inc., 2001
24. For similicity, the horizonal axis of Fig. 3 is plotted in $\lg P_O$. The linear dependence of $\ln P_O$ on $1/T_S$ as described in Eq. (2) remains in the plot since $\lg P_O = \lg e \cdot \ln P_O$.
25. M. B. Nielsen, D. Ceresoli, P. Parisiades, V. B. Prakapenka, T. Yu, Y. Wang, and M. Bremholm, Phase stability of the $SrMnO_3$ hexagonal perovskite system at high pressure and temperature, *Phys. Rev. B* 90(21), 214101 (2014)
26. L. Rørmark, A. B. Mørch, K. Wiik, S. Stølen, and T. Grande, Enthalpies of oxidation of $CaMnO_{3-\delta}$, $Ca_2MnO_{4-\delta}$ and $SrMnO_{3-\delta}$ deduced redox properties, *Chem. Mater.* 13(11), 4005 (2001)
27. S. Farokhipoor, C. Magén, S. Venkatesan, J. Íñiguez, C. J. M. Daumont, D. Rubi, E. Snoeck, M. Mostovoy, C. de Graaf, A. Müller, M. Döblinger, C. Scheu, and B. Noheda, Artificial chemical and magnetic structure at the domain walls of an epitaxial oxide, *Nature* 515(7527), 379 (2014)